PHDME: PHYSICS-INFORMED DIFFUSION MODELS WITHOUT EXPLICIT GOVERNING EQUATIONS

Anonymous authors

000

001

002 003 004

010 011

012

013

014

015

016

017

018

019

021

023

025

026

027

028

031

032

034

035

036

037

040

041

042

043

044

046

047

048 049

051

052

Paper under double-blind review

ABSTRACT

Diffusion models are expressive priors for generating and predicting data from high-dimensional dynamical systems. Yet, purely data-driven approaches often lack reliability and trustworthiness, motivating growing interest in physicsinformed machine learning (PIML). Most existing PIML methods, however, assume access to exact governing equations during training—an assumption that fails when the dynamics are unknown or too complex to model accurately. To address this gap, we introduce PHDME¹ (Port-Hamiltonian Diffusion Model), a physics-informed diffusion framework that learns system dynamics without requiring exact equations. Our approach first trains a Gaussian process distributed Port-Hamiltonian system (GP-dPHS) on limited observations to capture an energy-based representation of the dynamics. The GP-dPHS is then used to generate a physically consistent and diverse dataset for diffusion training. To enforce physics-consistency, we embed the GP-dPHS structure directly into the diffusion training objective through a loss that penalizes deviations from the learned Hamiltonian dynamics, weighted by the GP's predictive uncertainty. After training, we employ conformal prediction to provide distribution-free uncertainty quantification of the generated trajectories. In this way, PHDME is designed for regimes with scarce data and unknown equations, enabling data-efficient, physically valid trajectory generation with calibrated uncertainty estimates.

1 Introduction

Predicting the evolution of complex dynamical systems is central to policy design (Bevacqua et al., 2023), collision avoidance (Missura & Bennewitz, 2019), and long-horizon planning (Li et al., 2025). However, accurate forecasts remain a significant challenge where dynamics involve high nonlinearity and dimensionality, as well as when observational data are sparse and limited. A common constraint in robotics, for instance, where fully instrumenting a soft-bodied manipulator with tactile sensors is often expensive and physically difficult. Furthermore, many of these systems are described by partial differential equations (PDEs), but traditional numerical solvers are computationally expensive, which requires fine-grained spatiotemporal discretization that is overwhelming for real-time control or long-horizon forecasting. To tackle these challenges, various deep learning frameworks have been proposed to learn the underlying dynamics from collected data. Methods like neural ODE (Chen et al., 2018) and neural PDE (Zubov et al., 2021) formulations impose substantial computational cost. Training requires repeated forward time integrations together with backward sensitivity computations through stiff multiscale solvers. The computational cost scales up with prediction horizon, state dimension, and solver stiffness, leading to high runtime and memory usage that force compromises on model fidelity and spatial resolution of the grid. Although alternative frameworks, such as discrete-time autoregressive models, circumvent the integration cost, they introduce challenges of error accumulation over rollouts.

Diffusion models (Sohl-Dickstein et al., 2015) offer a flexible generative prior for forecasting in dynamical systems. Denoising diffusion defines a forward Markov corruption with Gaussian perturbations and trains a reverse process (Ho et al., 2020; Karras et al., 2022) that estimates the score of the data distribution, achieving state-of-the-art synthesis in images (Xia et al., 2023; Xu et al., 2023),

¹Code available at: https://github.com/InvincibleTdog/PHDME_anonymous

videos (Ho et al., 2022; Liang et al., 2024), and audio (Guo et al., 2024). In scientific machine learning the key advantage is the ability to represent full predictive distributions rather than single trajectories, which supports inverse problems (Chung et al., 2023) and planning (Römer et al., 2025) under uncertainty. In case of spatiotemporal problem that are encoded as an image 1 or video, the output of the diffusion model is the solution of the PDE over spatial and temporal domain. Nevertheless, standard diffusion models are purely data-driven, so samples may align with dataset statistics while violating the physics that govern the real world. The absence of explicit physics limits performance and reliability and weakens guarantees in applications like safety-critical systems (Tan et al., 2023).

Physics-informed training addresses this gap by constraining learning with governing equations. Classic work like physics-informed Neural Networks (PINNs) (Raissi et al., 2019) ensures that the learning outcomes follow the physics, and recent work has begun to embed such constraints into generative modeling (Shu et al., 2023; Bastek et al., 2024). These approaches typically require that the governing equations are known (except for some unknown parameters) and can be enforced during training. However, in many real systems, the exact governing equations are unknown or prohibitively complex to model, and observations are limited, e.g., modeling the equations of motion of soft robots via first principles is quite challenging due to the highly nonlinear and unstructured dynamics. Under these conditions, standard physics-informed pipelines are difficult to deploy.

Contribution: We are aiming at the topic of offering rapid, physically reliable, multi-step dynamic forecasting. In this paper, we propose PHDME, which is built on a Gaussian-process distributed Port-Hamiltonian System (Tan et al., 2024). The Port-Hamiltonian framework provides an expressive yet physically consistent representation for hard-to-model, unstructured dynamics. We learn the governing equations directly from limited observations by fitting a GP-dPHS that models the underlying Hamiltonian of the system. The learned GP-dPHS is then integrated into the diffusion training objective as a physics-consistency term that aligns the score network with Hamiltonian-consistent dynamics across noise levels. This coupling of energy-based representation learning with diffusion training enables data-efficient forecasting that respects physical structure even when governing equations are unavailable. Moreover, the probabilistic deep prior encapsulates a class of partial differential equations dynamics, enabling it to directly generate the PDE solution reliably even under unseen initial conditions, bypassing the need for iterative, numerical PDE solvers.

Our contributions can be summarized as:

- Leveraging a single draw from the diffusion model, PHDME provides fast forecasts for PDE systems where the governing equations are unknown but highly nonlinear. PHDME produces reliable results even the data availability is strictly limited.
- The proposed PHDME uses structured energy representations of the system to make the learning process physically informed. By using the Bayesian nature of the GP, diffusion model training has been weighted by the uncertainties from the data observation stage, which makes it possible to inform and constraint the system with physics without knowing the exact underlying functions.
- We also introduce a conformal prediction as postprocessing of the PHDME, where we
 not only provide a physically-valid sample given the initial condition, but also provide
 the uncertainty quantification of the sample. These features make the method suitable for
 safety-critical applications.

2 PRELIMINARY

In this section, we give a brief overview of denoise diffusion models, Gaussian process distributed Port-Hamiltonian systems, and conformal prediction (CP).

2.1 Denoising Diffusion Models

Diffusion models have demonstrated excellent potential in various domains (Ho et al., 2020; Song & Ermon, 2019; Dhariwal & Nichol, 2021). While recent efforts extend them to time series forecasting (Rasul et al., 2021), super resolution for dynamic prediction (Rühling Cachay et al., 2023), and time-invariant physics-informed generation (Bastek et al., 2024). The spatiotemporal forecasting

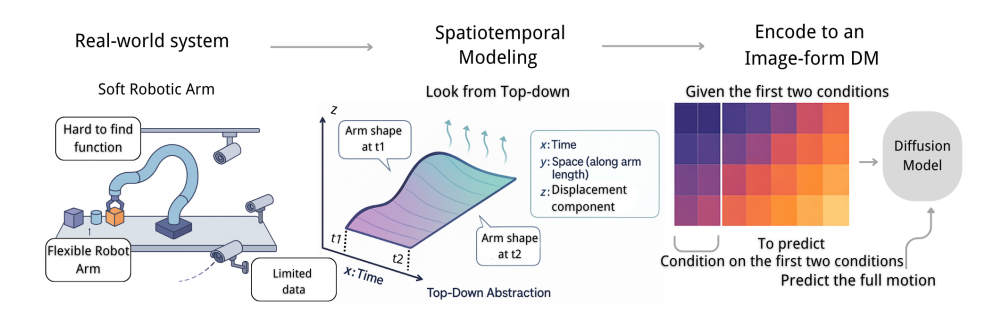


Figure 1: The left panel depicts a typical soft robot scenario in which a flexible continuum manipulator exhibits dynamics that are difficult to specify. The middle panel adopts a top-down parameterization with the y-axis as spatial projection along the arm direction, the z-axis (pixel value) as displacement, and the x-axis as temporal evolution. This converts the evolution into an image form, enabling the diffusion model to synthesize the full spatiotemporal field in a single shot rather than step-by-step rollouts.

with physics guarantee has remained underexplored, especially when the governing equations are unknown or difficult to obtain.

Diffusion indexing, parameterization, and objective. Let $A^{(m)}$ be the noised image at step $m \in \{0,\ldots,M\}$, where the diffusion step m is different to any physical time notation t. The forward noise corruption is linear Gaussian: $A^{(m)} = \alpha_m A^{(0)} + \sigma_m \varepsilon$ with $\varepsilon \sim \mathcal{N}(\mathbf{0},\mathbf{I})$; the schedule $\{(\alpha_m,\sigma_m)\}_{m=0}^M$ yields $A^{(M)} \approx \mathcal{N}(\mathbf{0},\mathbf{I})$. In the x_0 parameterization, a neural denoiser predicts the clean sample from a noised input and optional condition \mathbf{y} via $\widehat{A}^{(0)} = f_{\theta}([A^{(m)},\mathbf{y}],m)$. The reverse transition uses the closed-form Gaussian posterior with mean $\mu_m(A^{(m)},\widehat{A}^{(0)})$ and variance $\widetilde{\sigma}_m^2\mathbf{I}$, both fixed by the forward schedule. And w_m is set to Min-SNR-5 weighting (Hang et al., 2023). Training minimizes a timestep-weighted reconstruction loss

$$\mathcal{L}_{\text{DDPM}}(\theta) = \mathbb{E}_{m, \mathbf{A}^{(0)}, \boldsymbol{\varepsilon}} \left[w_m \| f_{\theta} ([\alpha_m \mathbf{A}^{(0)} + \sigma_m \boldsymbol{\varepsilon}, \mathbf{y}], m) - \mathbf{A}^{(0)} \|^2 \right].$$

Sampling and uncertainty. Starting from $A^{(M)} \sim \mathcal{N}(\mathbf{0}, \mathbf{I})$, generation iterates $A^{(m-1)} = \mu_m(A^{(m)}, \widehat{A}^{(0)}) + \tilde{\sigma}_m z$ with $z \sim \mathcal{N}(\mathbf{0}, \mathbf{I})$; repeated runs thus form an ensemble approximating the conditional distribution of $A^{(0)}$ given \mathbf{v} .

2.2 GAUSSIAN PROCESS DISTRIBUTED PORT-HAMILTONIAN SYSTEM

Based on Hamiltonian dynamics, GP-dPHS is a physics-informed PDE learning method that not only generalizes well from sparse data, but also provides uncertainty quantification (Tan et al., 2024). The composition of Hamiltonian systems through input and output ports leads to Port Hamiltonian systems, a class of dynamical systems in which ports formalize interactions among components. The Hamiltonian can also be interpreted as the energy representation of the system. This framework applies in the classical finite dimensional setting (Beckers et al., 2022) and extends naturally to distributed parameter and multivariable cases. In the infinite dimensional formulation, the interconnection, damping, and input and output matrices are replaced by matrix differential operators that do not explicitly depend on the state or energy variables. Under this learning structure, once the Hamiltonian is specified, the system model follows in a systematic manner. This general formulation is versatile enough to represent various PDEs and has been shown to capture a wide range of physical phenomena, including heat conduction, piezoelectricity, and elasticity. In what follows, we recall the definition of distributed Port Hamiltonian systems as presented in (Macchelli et al., 2004).

More formally, let \mathcal{Z} be a compact subset of \mathbb{R}^n representing the spatial domain, and consider a skew-adjoint constant differential operator J along with a constant differential operator G_d . Define the Hamiltonian functional $\mathcal{H} \colon \mathcal{X} \to \mathbb{R}$ in this following form:

$$\mathcal{H}(\boldsymbol{x}) = \int_{\mathcal{Z}} H(z, x) dV,$$

where $H\colon \times \mathcal{X} \to \mathbb{R}$ is the energy density. Denote by \mathcal{W} the space of vector-valued smooth functions on $\partial \mathcal{Z}$ representing the boundary terms $\mathcal{W} \coloneqq \{w|w = B_{\mathcal{Z}}(\delta_x \mathcal{H}, u)\}$ defined by the boundary operator $B_{\mathcal{Z}}$. Then, the general formulation of a multivariable dPHS Σ is fully described by

$$\Sigma(J, R, \mathcal{H}, G) = \begin{cases} \frac{\partial \mathbf{x}}{\partial t} = (J - R)\delta_{\mathbf{x}}\mathcal{H} + G_{d}\mathbf{u} \\ \mathbf{y} = G_{d}^{*}\delta_{\mathbf{x}}\mathcal{H} \\ w = B_{\mathcal{Z}}(\delta_{\mathbf{x}}\mathcal{H}, \mathbf{u}), \end{cases}$$
(1)

where R is a constant differential operator taking into account energy dissipation. Furthermore, $\boldsymbol{x}(t,\boldsymbol{z}) \in \mathbb{R}^n$ denotes the state (also called energy variable) at time $t \in \mathbb{R}_{\geq 0}$ and location $\boldsymbol{z} \in \mathcal{Z}$ and $\boldsymbol{u},\boldsymbol{y} \in \mathbb{R}^m$ the I/O ports, see (Tan et al., 2024) for more details. Generally, the J matrix defines the interconnection of the elements in the dPHS, whereas the Hamiltonian H characterizes their dynamical behavior. The constitution of the J matrix predominantly involves partial differential operators. The port variables \boldsymbol{u} and \boldsymbol{y} are conjugate variables in the sense that their duality product defines the energy flows exchanged with the environment of the system.

When the system dynamics are only partially known, the Hamiltonian can be modeled within a probabilistic framework using Gaussian processes. A Gaussian process is fully specified by a mean function and a covariance function, and as a nonparametric Bayesian prior, it is well-suited for smooth Hamiltonian functionals. Its invariance under linear transformations further supports consistent representation propagation through the operators that define the dynamics (Jidling et al., 2017).

Integrating these concepts, the unknown Hamiltonian latent function of a distributed system is encoded within a dPHS model to ensure physical consistency. Here, the unknown dynamics are captured by approximating the Hamiltonian functional with a GP, while treating the matrices J,R, and G (more precisely, their estimates $\hat{J}_{\Theta}, \hat{R}_{\Theta}$, and \hat{G}_{Θ}) as hyperparameters. This leads to the following GP representation for the system dynamics:

$$\frac{\partial \boldsymbol{x}}{\partial t} \sim \mathcal{GP}(\hat{G}_{\Theta}\boldsymbol{u}, k_{dphs}(\boldsymbol{x}, \boldsymbol{x}')),$$

with a physics-informed kernel function defined as

$$k_{dphs}(\boldsymbol{x}, \boldsymbol{x}') = \sigma_f^2(\hat{J}\hat{R}_{\Theta})\delta_{\boldsymbol{x}} \exp\left(-\frac{\|\boldsymbol{x} - \boldsymbol{x}'\|^2}{2\varphi_l^2}\right)\delta_{\boldsymbol{x}'}^{\top}(\hat{J}\hat{R}_{\Theta})^{\top},$$

where $\hat{J}R_{\Theta}=\hat{J}_{\Theta}-\hat{R}_{\Theta}$ and the kernel is based on the squared exponential function. The training of this GP-dPHS model involves optimizing the hyperparameters Θ , φ_l , and σ_f by minimizing the negative log marginal likelihood. Hence, the physics representation prior is learned by GP without any presumption of the functional form; this information is fully described by the structured mean function and variance function.

Exploiting the linear invariance property of GPs, the Hamiltonian $\hat{\mathcal{H}}$ now follows a GP prior. This integration effectively combines the structured, physically consistent representation of distributed Port-Hamiltonian systems with the flexibility of GP to handle uncertainties and learn unknown dynamics from data. The resulting framework not only ensures that the model adheres to the underlying physics but also provides a comprehensive, data-informed prediction of the system's behavior.

2.3 CONFORMAL PREDICTION

Conformal prediction a statistical technique used to quantify the uncertainty of predictions in machine learning models. It provides a prediction set that contains the true output with a user-specified probability $1-\delta$. We calibrate the mean squared error of our stochastic generator with conformal prediction. Let the calibration set be $\mathcal{D}_{\text{cal}} = \left\{\mathbf{x}_i^{\star}\right\}_{i=1}^{K}$, where each \mathbf{x}_i^{\star} is the ground-truth dynamic landscape on the grid \mathcal{G} . For every i we call the predictor Num times, drawing $\widehat{\mathbf{x}}_i^{(n)} \sim \mathsf{P}_{\theta}(\cdot)$, $n=1,\ldots,N$, and define the non-conformity score (NCS) of a single sample as (Lindemann et al., 2023; Vlahakis et al., 2024):

$$r_{i,n} = \frac{1}{|\mathcal{G}|} \left\| \widehat{\mathbf{x}}_i^{(n)} - \mathbf{x}_i^{\star} \right\|_F^2.$$
 (2)

Pooling the K*Num scores and sorting them in ascending order gives an empirical error distribution for a single stochastic draw. For a target miscoverage level $\delta \in (0,1)$, set the calibrated threshold to the order statistic

$$\tau := \text{Quantile}_{(1 + \frac{1}{K * Num})(1 - \delta)}(r^{(1)}, \dots, r^{(K * Num)}), \tag{3}$$

Under exchangeability of scores, we can say under at least $1 - \delta$ probability guarantee, a future prediction from $P_{\theta}(\cdot)$ has mean squared error at most τ_{δ} , formally as: $\mathbb{PROB}(r \leq \tau) \geq 1 - \delta$.

3 PROPOSED PHDME

In this section, we will discuss the assumptions and problem formulation, followed by a detailed introduction of the proposed Port-Hamiltonian Diffusion Model without Explicit underlying equations (PHDME) enhances predictive performance by leveraging the learned energy representations and observation uncertainties.

3.1 Assumptions and Settings

We study the problem of spatiotemporal dynamic prediction with uncertainty quantification. We have a PDE system $0 = f(\mathbf{x}, \mathbf{dx}, \cdots)$ and aim to predict the solution for $t = 0, \cdots, T$ for this system. We assume that this system can be written in dPHS form even though we do not require knowledge about the components. further we assume that we can collect limited data from the PDE.

Hence, instead of learning the regular dynamic directly, where the underlying functions are hard to acquire. We transform the problem space to the structured derivative space. The energy representation can be modeled through a distributed Port-Hamiltonian system. We adopt a dPHS representation in which the dynamics are modeled as

$$\frac{\partial \boldsymbol{x}}{\partial t} = (J - R)\delta_{\boldsymbol{x}}\hat{\mathcal{H}} + G_d\boldsymbol{u}$$

where J is power preserving, R is dissipative, G_d maps inputs, and $\hat{\mathcal{H}}$ is a learned Hamiltonian functional. In PHDME, $\hat{\mathcal{H}}$ is represented by a Gaussian process trained on limited observations, and the induced Hamiltonian gradients are integrated into the diffusion training objective through a physics consistency term. This aligns the learned score field with Hamiltonian consistent dynamics across noise levels and avoids reliance on guidance during sampling.

We make the following assumptions:

Assumption 1 The PHDME is designed to handle the scenario where the observations are limited and the underlying functions are hard to acquire, which means the regular data-driven predictors are hard to train and the conventional physics-informed methods are not able to handle. We observe the state on a limited spatiotemporal grid, yielding measurements $\left\{ \boldsymbol{x}(t_i, z_j) \right\}_{i=1,\dots,N_t}^{j=1,\dots,N_z}$.

Assumption 2 The structural form of the interconnection, dissipation, and input operators is known up to a finite set of parameters. Specifically, J, R, and G_d are specified by templates with unknown coefficients $\Theta \subset \mathbb{R}^{n_{\Theta}}$, which are estimated from data. The qualitative structure, such as the type of friction model encoded in R, is known, while the numerical values of the parameters may be unknown.

3.2 PHDME FRAMEWORK

Instead of forecasting by sequential rollouts or numerical integration, which can be computationally expensive, PHDME generates the entire future spatiotemporal field in a single pass conditioned on the given initial conditions. The central idea is to guide this single draw-image like generation with a deep prior learned from limited observations. The training pipeline has two stages, as illustrated in Figure 2. First, we encode the scarce observations from the real system through the dPHS structure. And naturally learn a probabilistic energy-based representation of the system using the Gaussian processes. Then this deep prior is used to synthesize a rich dataset for the diffusion model training, as well as guiding the second training stage of the PHDME with a physics consistency loss derived from the prior and weighted by its predictive uncertainty based on observations, thereby aligning the learned score field with Hamiltonian consistent dynamics while preserving data efficiency.

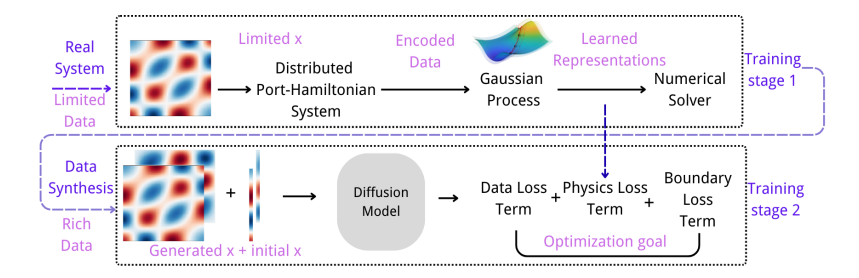


Figure 2: This figure visualize the two-stage training of the PHDME, where we firstly train a rather slow but structured deep prior. Then we leverage this prior to inform the diffusion training for rapid sample generations.

Data collection and GP-dPHS training (stage 1). We observe the state $\mathbf{x}(t,z)$ at discrete times and spatial locations, $\mathcal{D} = \left\{t_i, \ z_j, \ \mathbf{x}(t_i,z_j), \ u(t_i)\right\}_{i=0,j=0}^{i=N_t-1,j=N_z-1}$. Since measurements are sparse and derivatives are required for model learning, we fit a smooth Gaussian process interpolant to x(t,z) using a squared exponential kernel, and exploit closed form differentiation of the Gaussian process to collect over time yields $X = \left[\tilde{x}(t_0), \dots, \tilde{x}(t_{N_t-1})\right], \dot{X} = \left[\partial_t \tilde{x}(t_0), \dots, \partial_t \tilde{x}(t_{N_t-1})\right],$ and the training set $\mathcal{E} = \left[X, \dot{X}\right]$, aligned with the input sequence $\left\{u(t_i)\right\}_{i=1}^{N_t}$. This construction provides derivative information from x(t,z) while enlarging spatial coverage for subsequent GP dPHS training. Based on this dataset, we learn a distributed Port Hamiltonian representation in which the dynamics satisfy

$$\partial_t \boldsymbol{x}(t,z) = (J-R)\,\delta_{\boldsymbol{x}}\hat{\mathcal{H}}(t,z) + G_d\,\boldsymbol{u}(t,z),$$

with interconnection matrix J, dissipative term R, and Hamiltonian $\hat{\mathcal{H}}$. The unknown Hamiltonian is modeled by a Gaussian process and eventually unknown coefficients of J, R, and G_d are treated as hyperparameters Θ . Using the linear invariance of Gaussian processes, we place a GP prior on the energy derivatives and obtain a GP over the time derivative of the state,

$$\partial_t \boldsymbol{x} \sim \mathcal{GP}(\hat{G}_{\Theta} \boldsymbol{u}, k_{dphs}(\boldsymbol{x}, \boldsymbol{x}')),$$

with physics-informed kernel

$$k_{dphs}(\boldsymbol{x}, \boldsymbol{x}') = \sigma_f^2 \left(\hat{J}_{\Theta} - \hat{R}_{\Theta} \right) \delta_{\boldsymbol{x}} \exp \left(- \frac{\|\boldsymbol{x} - \boldsymbol{x}'\|^2}{2\varphi_l^2} \right) \delta_{\boldsymbol{x}'}^{\top} \left(\hat{J}_{\Theta} - \hat{R}_{\Theta} \right)^{\top}.$$

We train the model on $\mathcal E$ by maximizing the marginal likelihood with respect to Θ and the kernel hyperparameters (φ_l, σ_f) . The resulting posterior induces a stochastic Hamiltonian $\hat{\mathcal H}$ and yields the learned dPHS

$$\partial_t \boldsymbol{x}(t,z) = (\hat{J}_{\Theta} - \hat{R}_{\Theta}) \, \delta_{\boldsymbol{x}} \hat{\mathcal{H}}(t,z) + \hat{G}_{\Theta} \, \boldsymbol{u}(t,z),$$

which serves as a probabilistic physics prior for subsequent data generation and diffusion training. However, since this numerical solution of GP-dPHS is computational demanding, we train a physics-informed diffusion model instead of directly using the GP-dPHS for prediction.

Dataset generation using GP samples. We place a GP prior over the energy functional, yielding a posterior that captures a family of plausible energy representations. Using only the posterior mean to represent the learned dynamics neglects posterior uncertainty and is therefore not a valid surrogate for the true system. Instead, we leverage random fourier feature prior draw to provide realizations of the GP-dPHS that will be used as training data for the diffusion model. See appendix A.3 for more details.

GP-dPHS yields a posterior over Hamiltonian energy functionals rather than a single estimate based on limited observations, as discussed in 3.2. We draw function realizations of the Hamiltonian gradient $\delta_x \hat{\mathcal{H}}$ from this posterior and then plug it into the dPHS form and solve it numerically to generate a trajectory $\mathbf{x}(z,t)$. For a real and shift-invariant kernel k_f , Bochner theory (Langlands, 2006) implies a spectral density that admits a finite feature approximation. We use a random feature map:

$$\phi(\mathbf{x}) = \sqrt{\frac{2}{d}} \left[\cos(\boldsymbol{\omega}_1^{\mathsf{T}} \mathbf{x} + \beta_1), \dots, \cos(\boldsymbol{\omega}_D^{\mathsf{T}} \mathbf{x} + \beta_D) \right]^{\mathsf{T}},$$

 with ω_j drawn from the spectral density and $\beta_j \sim \text{Uniform}[0, 2\pi]$. The d denotes the dimensions of the feature map, so that $k_f(\mathbf{x}, \mathbf{x}') \approx \phi(\mathbf{x})^\top \phi(\mathbf{x}')$. A pathwise prior sample is

$$f(\mathbf{x}) = \phi(\mathbf{x})^{\top} \mathbf{w}, \quad \mathbf{w} \sim \mathcal{N}(\mathbf{0}, \mathbf{I}),$$

which provides one realization for the stacked gradients $\delta_{\boldsymbol{x}}\mathcal{H}$. Then the posterior correction on a finite set can be occupied. For any query set $X = [\mathbf{x}^{\star}(t_0), \dots, \mathbf{x}^{\star}(t_{N_t-1})]$, define the covariance kernel: $\mathbf{C}_{XX} = [k_f(\mathbf{x}_i, \mathbf{x}_j)]_{ij}$, $\mathbf{C}_{\star X} = [k_f(\mathbf{x}_i^{\star}, \mathbf{x}_j)]_{ij}$. A posterior function sample on X_{\star} is then

$$f(\mathbf{x}^{\star}) = \mu_f(\mathbf{x}^{\star}) + f(\mathbf{x}^{\star}) + \mathbf{C}_{\star X} (\mathbf{C}_{XX} + \sigma_n^2 \mathbf{I})^{-1} (\mathbf{y} - \mu_f(X) - f(X)),$$

applied component wise to $\delta_x \mathcal{H}$. This warps the prior draw to match the observations and yields an exact finite dimensional posterior sample suitable for insertion into the dPHS evolution. By evaluating the sample-based posterior function under different initial conditions, we build a rich training and validation set for the PHDME.

Diffusion training Notation. We follow the diffusion indexing introduced above. The latent at diffusion step $m \in \{0, \dots, M\}$ is $\mathbf{A}^{(m)}$, the clean tensor is $\mathbf{A}^{(0)}$, and conditioning is provided by the first two frames \mathbf{c}_{init} . The denoiser f_{θ} predicts the clean tensor in the \mathbf{A}_0 parameterization,

$$\widehat{\boldsymbol{A}}^{(0)} = f_{\theta}([\boldsymbol{A}^{(m)}, \mathbf{c}_{\text{init}}], m).$$

We interpret $\widehat{\boldsymbol{A}}^{(0)}$ as the image like representation of the state over the spatiotemporal grid $\mathcal{T} \times \mathcal{Z}$, where $\mathcal{T} = \left\{ t_0, \, \cdots, \, t_i \, \right\}_{i=0}^{i=N_t-1}$. and $\mathcal{Z} = \left\{ z_0, \, \cdots, \, z_j \, \right\}_{j=0}^{j=N_z-1}$. aligned with \mathbf{c}_{init} .

Physics operator from GP dPHS. Since data-driven methods always compromise their reliability, we follow the idea of (Bastek et al., 2024) to include physics in the loss functions; however, we learn the deep probabilistic physics priors to inform the model of physics instead of the governing equations. Let $\delta_{\boldsymbol{x}}\hat{\mathcal{H}} = [\partial\hat{\mathcal{H}}/\partial p,\ \partial\hat{\mathcal{H}}/\partial q]^{\top}$ denote the Hamiltonian gradients provided by the trained Gaussian process distributed Port Hamiltonian model, and let J and R be the interconnection and dissipation operators. On the discrete grid we evaluate the dPHS residual on a candidate field \boldsymbol{x} implied by $\widehat{\boldsymbol{A}}^{(0)}$ and \mathbf{c}_{init} , recall equations in 1 as $\mathcal{F}_{\text{phys}}$, we use centered differences in the interior

implied by $A^{(0)}$ and c_{init} , recall equations in 1 as $\mathcal{F}_{\text{phys}}$, we use centered differences in the interior and consistent boundary stencils. We aggregate this residual into a scalar penalty with boundary terms,

$$\mathcal{R}_{\text{phys}}(\widehat{\boldsymbol{A}}^{(0)}; \mathbf{c}_{\text{init}}) = \frac{1}{|\Omega|} \| \mathcal{F}_{\text{dPHS}}(\boldsymbol{x}) \|_{2}^{2} + \lambda_{\text{bc}} \mathcal{B}(\boldsymbol{x}; \mathbf{c}_{\text{init}}). \tag{4}$$

We weight the contribution of each grid location by the Gaussian process posterior variance to obtain an uncertainty aware version $\widetilde{\mathcal{R}}_{phys}$ adjusting by a variance factor Ω in 4. This implies that representation learning has considered the impacts of observation uncertainties, see A.5 for details.

PHDME training objective. PHDME augments the standard reconstruction objective with the physics penalty evaluated on the denoised prediction,

$$\mathcal{L}_{\mathrm{PHDME}}(\theta) = \mathbb{E}_{m, \mathbf{A}^{(0)}, \mathbf{\varepsilon}} \left[w_m \left\| f_{\theta} \left([\mathbf{A}^{(m)}, \mathbf{c}_{\mathrm{init}}], m \right) - \mathbf{A}^{(0)} \right\|_2^2 + \lambda_{\mathrm{phys}} \widetilde{\mathcal{R}}_{\mathrm{phys}} \left(f_{\theta} ([\mathbf{A}^{(m)}, \mathbf{c}_{\mathrm{init}}], m); \mathbf{c}_{\mathrm{init}} \right) \right].$$

The second term backpropagates through f_{θ} and aligns the learned score field with Hamiltonian consistent dynamics across diffusion steps. It does not alter the forward noising process or the ancestral form of the reverse kernel. The physics loss term

Generative uncertainty based on conformal prediction. In dynamic generation, we require not only physically correct structure but also calibrated generative uncertainty to assess forecast reliability. We adopt sample-based conformal prediction as a postprocessing step, see Section 2.3. The reverse diffusion in DDPM is stochastic, which supports the exchangeability assumption of conformal prediction. We therefore construct a calibration set and a test set to quantify the uncertainty of samples produced by PHDME. Hence, we construct the calibration set based on the non-conformity score calculated based on K initial conditions and Num stochastic calls of the PHDME based on each one of them. Recall the formally defined score in 2. The calibration set $\mathcal{D}_{\text{cal}} = \left\{ (\mathbf{c}_{\text{init}}^{(i)}, \mathbf{x}_i^{\star}) \right\}_{i=1}^K$ is able to offer a calibrated threshold τ under $1 - \delta$ success rate, this quantile can be formally defined as equation 3. And for future testing and generation, we construct the on-the-fly test set. And it holds that: $\mathbb{PROB}(r \leq \tau_{\delta}) \geq 1 - \delta$.

4 EXPERIMENTS

In this section, we demonstrate the effectiveness and performance of the PHDME. By quantitatively discuss the accuracy and generative speed, and qualitatively visualizing the generated sample, we show the powerful aspects of the framework. The further discussion can be found in the appendix.

4.1 SETUP

PHDME is designed for application scenarios where underlying functions are hard to acquire, for example, soft robots, flexible cable construction, oil drilling, etc. We evaluate the model using a physically faithful simulator of a fixed-end string that solves the one-dimensional wave equation on a fine grid and then projects to the learning grid. This soft string approximates the highly nonlinear PDE dynamics of the soft robots, see appendix A.1 for more calculation details. Due to the complexities in various initial shapes and magnitudes of the momentum, the traditional data-driven method always requires a huge observation set to train the model sufficiently. However, we only offer 20 samples on the 64×64 grid as the observation set and add a downsample factor of 50 to address the data collection challenge. We leverage this downsampled data to train the GP-dPHS, using GP sample 3.2 to synthesize a training and validation set of 10000 and 1000 data samples, respectively. In addition, we leverage the simulator to create 10000 data samples as the real-world test set to comapre the trained models to the real-world system. By solving the PDE using the GP priors on a 64×64 grid, PHDME generate the dynamic landscape. We utilize the U-Net (Ronneberger et al., 2015) architecture with 64×64 pixels as I/O dimensions that align with the considered grid. And use the 4-channel design where two are used for conditioning, and the others are leveraged for correlated dynamic generations.

Baselines. Recalling the assumption 1 that underlying functions are hard to acquire, which is a widely existing and non-trivial realistic setting. The normal function-based physics-informed generative models (Jacobsen et al., 2025; Bastek et al., 2024) are no longer available in this case. Hence, we set the baselines using the data-driven diffusion model and diffusion model with limited access to the underlying physics, which is assumed to know the fixed boundary conditions that is easy to be observed, to prove that our single-shot dynamic generations excel in terms of forecasting accuracy, while keeping the predictor physically-informed and uncertainty-aware. We also compare the generative speed against the step-by-step predictor GP-dPHS, showing our fast forecast potentials.

4.2 RESULTS

Quantitative results We present the grid-average metrics for the nonlinear string PDEs in Table 4.2 and visualize the testing on the real world data in Figure 3

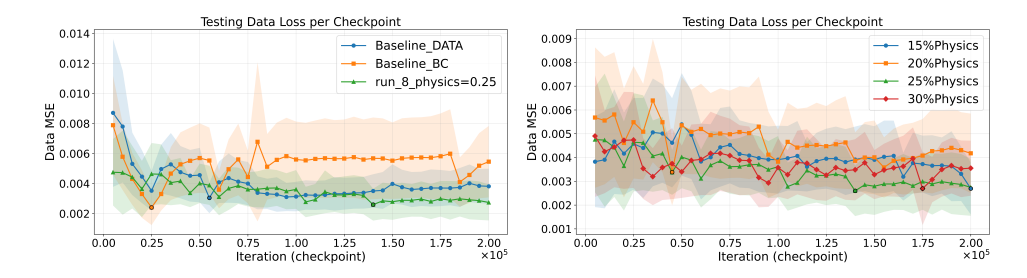


Figure 3: On the left side, PHDME beats the baselines with pure-data driven and limited physics access by having the minimum MSE over iterations. On the right side, we further investigate the potential impacts of the physics-loss term percentage regarding the performance.

We select the best model trained based on the validation on the synthesis dataset, and test its performance by measuring the MSE and generative uncertainties based on conformal prediction. Based on the quantified error and non-conformalty score, the proposed PHDME beats both baselines, boasting its advantages when facing the unseen initial conditions and environments. This also proves the physics-informed method's potential for better generalization with reliability. And

Metrics	Test on Real-World Data		
	PHDME	DDPM	DDPM+Limited Physics
MSE NCS	$0.00274 \pm 1.42\mathrm{e}{-6} \\ 6.41\mathrm{e}{-3}$	$0.00381 \pm 1.37e - 6$ 6.82e - 6	$0.00546 \pm 5.66e - 6$ 9.80e - 3
Metrics	Forecast Time Comparision		
	PHDME		GP-dPHS (step-by-step model)
Time(s)	2.89		56.46

Table 1: Test performance (mean \pm var). Lower is better for Mean Squared Error (MSE)/non-conformity score (NCS). Representing accurate generation with smaller generative error boundary. And the generative time of the proposed PHDME is significantly higher than the GP-dPHS

the non-conformity score (NCS) for PHDME is also lower under 90% guarantees. The resulting tighter conformal bounds indicate sharper yet well-calibrated predictions, supporting reliability under stochastic sampling and improved generalization to previously unseen conditions. The baseline configurations, which remove either the physics structure or the uncertainty weighting, serve as natural **ablations** under the same training and evaluation protocol; the observed performance gap demonstrates that the physics-informed design materially improves both accuracy and calibrated uncertainty. We have a more detailed discussion in the appendix.

Qualitative results We qualitatively assess the full PHDME pipeline by inspecting predicted states. Our success criterion is accurate state forecasting under unseen initial conditions and environments. As illustrated in Fig. 4.2, generated samples closely match the true system behavior, preserving boundary behavior and phase progression. See (App. A.4) that errors introduced by the GP-dPHS data generation and by diffusion sampling are both limited on the evaluation grid. Taken together, these results indicate that the learned representation captures the underlying dynamics in the joint state/derivative space and supports reliable generation of the PDE system.

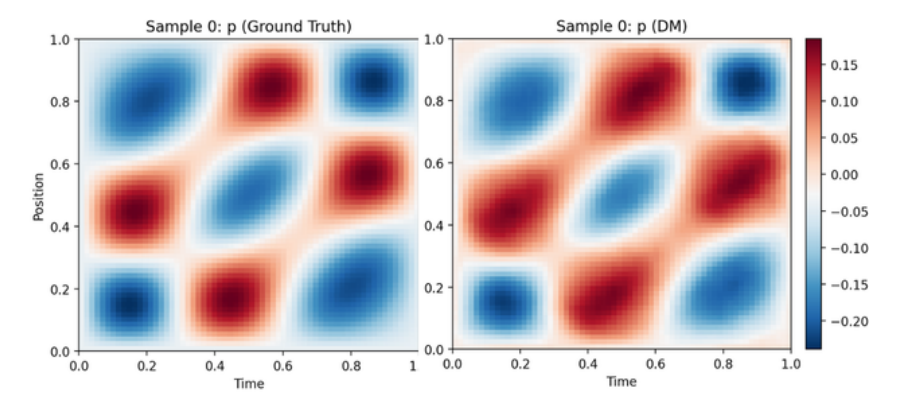


Figure 4: Left: Ground-truth state evolution of the wave equation. Right: Physically consistent and accurate prediction of PHDME based on sparse data and limited knowledge of the governing equations. Key takeaway: PHDME generates samples with correct dynamic pattern and amplitude by only conditioning on the initial two frames.

5 CONCLUSION

We presented a physics-informed diffusion framework that couples a GP-dPHS surrogate with a conditional denoising diffusion model to provide fast and physically reliable predictions for partially unknown PDE systems. The surrogate provides a distribution over admissible energy representations rather than a point estimate and the diffusion model learns to map noisy latents to clean fields while respecting this structure. Uncertainty quantification is addressed by distribution-free conformal prediction, On a synthetic PDE benchmark with unseen initial condition, the method improves accuracy and produces tighter conformal thresholds at the target coverage level, indicating better generalization relative to non-physics and ablated baselines.

REFERENCES

- Jan-Hendrik Bastek, WaiChing Sun, and Dennis M Kochmann. Physics-informed diffusion models. *arXiv preprint arXiv:2403.14404*, 2024.
- Thomas Beckers, Jacob Seidman, Paris Perdikaris, and George J Pappas. Gaussian process porthamiltonian systems: Bayesian learning with physics prior. In 2022 IEEE 61st Conference on Decision and Control (CDC), pp. 1447–1453. IEEE, 2022.
- Emanuele Bevacqua, Laura Suarez-Gutierrez, Aglaé Jézéquel, Flavio Lehner, Mathieu Vrac, Pascal Yiou, and Jakob Zscheischler. Advancing research on compound weather and climate events via large ensemble model simulations. *Nature Communications*, 14(1):2145, 2023.
- Ricky TQ Chen, Yulia Rubanova, Jesse Bettencourt, and David K Duvenaud. Neural ordinary differential equations. *Advances in neural information processing systems*, 31, 2018.
- Hyungjin Chung, Dohoon Ryu, Michael T McCann, Marc L Klasky, and Jong Chul Ye. Solving 3d inverse problems using pre-trained 2d diffusion models. In *Proceedings of the IEEE/CVF conference on computer vision and pattern recognition*, pp. 22542–22551, 2023.
- Prafulla Dhariwal and Alexander Nichol. Diffusion models beat gans on image synthesis. *Advances in neural information processing systems*, 34:8780–8794, 2021.
- Zhifang Guo, Jianguo Mao, Rui Tao, Long Yan, Kazushige Ouchi, Hong Liu, and Xiangdong Wang. Audio generation with multiple conditional diffusion model. In *Proceedings of the AAAI Conference on Artificial Intelligence*, volume 38, pp. 18153–18161, 2024.
- Tiankai Hang, Shuyang Gu, Chen Li, Jianmin Bao, Dong Chen, Han Hu, Xin Geng, and Baining Guo. Efficient diffusion training via min-snr weighting strategy. In *Proceedings of the IEEE/CVF international conference on computer vision*, pp. 7441–7451, 2023.
- Jonathan Ho, Ajay Jain, and Pieter Abbeel. Denoising diffusion probabilistic models. *Advances in neural information processing systems*, 33:6840–6851, 2020.
- Jonathan Ho, Tim Salimans, Alexey Gritsenko, William Chan, Mohammad Norouzi, and David J Fleet. Video diffusion models. *Advances in neural information processing systems*, 35:8633–8646, 2022.
- Christian Jacobsen, Yilin Zhuang, and Karthik Duraisamy. Cocogen: Physically consistent and conditioned score-based generative models for forward and inverse problems. *SIAM Journal on Scientific Computing*, 47(2):C399–C425, 2025.
- Carl Jidling, Niklas Wahlström, Adrian Wills, and Thomas B Schön. Linearly constrained Gaussian processes. *Advances in Neural Information Processing Systems*, 30, 2017.
- Tero Karras, Miika Aittala, Timo Aila, and Samuli Laine. Elucidating the design space of diffusion-based generative models. *Advances in neural information processing systems*, 35:26565–26577, 2022.
- Robert P Langlands. Problems in the theory of automorphic forms to salomon bochner in gratitude. In *Lectures in modern analysis and applications III*, pp. 18–61. Springer, 2006.
- Peilun Li, Kaiyuan Tan, and Thomas Beckers. Napi-mpc: Neural accelerated physics-informed mpc for nonlinear pde systems. In 7th Annual Learning for Dynamics\& Control Conference, pp. 1230–1242. PMLR, 2025.
- Jingyun Liang, Yuchen Fan, Kai Zhang, Radu Timofte, Luc Van Gool, and Rakesh Ranjan. Movideo: Motion-aware video generation with diffusion model. In *European Conference on Computer Vision*, pp. 56–74. Springer, 2024.
- Lars Lindemann, Matthew Cleaveland, Gihyun Shim, and George J Pappas. Safe planning in dynamic environments using conformal prediction. *IEEE Robotics and Automation Letters*, 8(8): 5116–5123, 2023.

- Alessandro Macchelli, Arjan J Van Der Schaft, and Claudio Melchiorri. Port Hamiltonian formulation of infinite dimensional systems i. modeling. In 2004 43rd IEEE Conference on Decision and Control (CDC), volume 4, pp. 3762–3767. IEEE, 2004.
 - Marcell Missura and Maren Bennewitz. Predictive collision avoidance for the dynamic window approach. In 2019 International Conference on Robotics and Automation (ICRA), pp. 8620–8626. IEEE, 2019.
 - Maziar Raissi, Paris Perdikaris, and George E Karniadakis. Physics-informed neural networks: A deep learning framework for solving forward and inverse problems involving nonlinear partial differential equations. *Journal of Computational physics*, 378:686–707, 2019.
 - Kashif Rasul, Calvin Seward, Ingmar Schuster, and Roland Vollgraf. Autoregressive denoising diffusion models for multivariate probabilistic time series forecasting. In *International conference on machine learning*, pp. 8857–8868. PMLR, 2021.
 - Ralf Römer, Alexander von Rohr, and Angela Schoellig. Diffusion predictive control with constraints. In 7th Annual Learning for Dynamics\& Control Conference, pp. 791–803. PMLR, 2025.
 - Olaf Ronneberger, Philipp Fischer, and Thomas Brox. U-net: Convolutional networks for biomedical image segmentation. In *International Conference on Medical image computing and computer-assisted intervention*, pp. 234–241. Springer, 2015.
 - Salva Rühling Cachay, Bo Zhao, Hailey Joren, and Rose Yu. Dyffusion: A dynamics-informed diffusion model for spatiotemporal forecasting. *Advances in neural information processing systems*, 36:45259–45287, 2023.
 - Dule Shu, Zijie Li, and Amir Barati Farimani. A physics-informed diffusion model for high-fidelity flow field reconstruction. *Journal of Computational Physics*, 478:111972, 2023.
 - Jascha Sohl-Dickstein, Eric Weiss, Niru Maheswaranathan, and Surya Ganguli. Deep unsupervised learning using nonequilibrium thermodynamics. In *International conference on machine learn*ing, pp. 2256–2265. pmlr, 2015.
 - Yang Song and Stefano Ermon. Generative modeling by estimating gradients of the data distribution. *Advances in neural information processing systems*, 32, 2019.
 - Kaiyuan Tan, Jun Wang, and Yiannis Kantaros. Targeted adversarial attacks against neural network trajectory predictors. In *Learning for Dynamics and Control Conference*, pp. 431–444. PMLR, 2023.
 - Kaiyuan Tan, Peilun Li, and Thomas Beckers. Physics-constrained learning of pde systems with uncertainty quantified port-hamiltonian models. In *6th Annual Learning for Dynamics & Control Conference*, pp. 1753–1764. PMLR, 2024.
 - Eleftherios E Vlahakis, Lars Lindemann, Pantelis Sopasakis, and Dimos V Dimarogonas. Conformal prediction for distribution-free optimal control of linear stochastic systems. *IEEE Control Systems Letters*, 2024.
 - Bin Xia, Yulun Zhang, Shiyin Wang, Yitong Wang, Xinglong Wu, Yapeng Tian, Wenming Yang, and Luc Van Gool. Diffir: Efficient diffusion model for image restoration. In *Proceedings of the IEEE/CVF international conference on computer vision*, pp. 13095–13105, 2023.
 - Xingqian Xu, Zhangyang Wang, Gong Zhang, Kai Wang, and Humphrey Shi. Versatile diffusion: Text, images and variations all in one diffusion model. In *Proceedings of the IEEE/CVF international conference on computer vision*, pp. 7754–7765, 2023.
 - Kirill Zubov, Zoe McCarthy, Yingbo Ma, Francesco Calisto, Valerio Pagliarino, Simone Azeglio, Luca Bottero, Emmanuel Luján, Valentin Sulzer, Ashutosh Bharambe, Nand Vinchhi, Kaushik Balakrishnan, Devesh Upadhyay, and Chris Rackauckas. Neuralpde: Automating physics-informed neural networks (pinns) with error approximations, 2021. URL https://arxiv.org/abs/2107.09443.

A APPENDIX

A.1 GROUND-TRUTH PDE DATA GENERATION

We synthesize supervision using a physically faithful simulator of a fixed-end string that solves the one-dimensional wave equation on a fine grid and then projects to the learning grid. Let s(z,t) denote displacement, with spatial domain $z \in [0,L]$ and time $t \in [0,T]$. The continuous dynamics satisfy

$$\partial_{tt}s(z,t) = c^2 \,\partial_{zz}s(z,t), \qquad s(0,t) = 0, \ s(L,t) = 0,$$
 (5)

with initial conditions $s(z,0) = s_0(z)$ and $\partial_t s(z,0) = w_0(z)$. The learned state is the derivative pair

$$p(z,t) = \partial_z s(z,t), \qquad q(z,t) = \partial_t s(z,t),$$
 (6)

and we collect the state vector as $\mathbf{x}(z,t) = [p(z,t), q(z,t)].$

Fine-to-coarse simulation. We integrate an equivalent first-order system on a fine grid and then downsample to the learning resolution. Let $y(t) = [s(\cdot,t);\ w(\cdot,t)]$ with $w = \partial_t s$. Discretize space on $N_z^{\rm fine}$ nodes with step $\Delta z^{\rm fine}$, and approximate the Laplacian by a second-order central stencil. The semi-discrete dynamics are

$$\frac{\mathrm{d}}{\mathrm{d}t} \begin{bmatrix} s \\ w \end{bmatrix} = \begin{bmatrix} w \\ c^2 \mathbf{D}_{\text{fine}}^{zz} s \end{bmatrix}, \qquad s_1(t) = s_{N_z^{\text{fine}}}(t) = 0, \tag{7}$$

where $\mathbf{D}_{\mathrm{fine}}^{zz}$ is the tridiagonal second–difference operator with Dirichlet boundary rows. We integrate (7) over N_t^{fine} fine time points using an adaptive ODE solver. From the fine solution we compute

$$p^{\text{fine}} = \partial_z s \approx \mathbf{D}_{\text{fine}}^z s, \qquad q^{\text{fine}} = \partial_t s \approx \mathbf{D}_{\text{fine}}^t s,$$
 (8)

with $\mathbf{D}_{\mathrm{fine}}^z$ the centered first–difference in z and $\mathbf{D}_{\mathrm{fine}}^t$ a centered time stencil. Optional Gaussian smoothing with standard deviation σ may be applied to s before differencing. We then downsample $(p^{\mathrm{fine}},q^{\mathrm{fine}})$ to the learning grid of size $N_z \times N_t$ to obtain

$$p \in \mathbb{R}^{N_z \times N_t}, \qquad q \in \mathbb{R}^{N_z \times N_t}.$$
 (9)

Randomized, valid initial conditions. To span smooth, physically consistent excitations, we sample s_0 and w_0 as finite Fourier–sine series that respect fixed ends:

$$s_0(z) = \sum_{n=1}^{N_{\rm m}} a_n \sin\left(\frac{n\pi z}{L}\right) \cos\phi_n, \qquad w_0(z) = \sum_{n=1}^{N_{\rm m}} a_n \sin\left(\frac{n\pi z}{L}\right) \sin\phi_n \frac{n\pi c}{L}, \tag{10}$$

with amplitudes a_n in a symmetric range and phases $\phi_n \sim \mathcal{U}[0, 2\pi)$.

Four-channel tensor with boundary conditioning. Each sample is packaged into

$$\left[\text{p_field, full_p, q_field, full_q} \right] \in \mathbb{R}^{4 \times N_z \times N_t},$$

where full-p = p and full-q = q. The conditioning channels encode the first two time frames with zeros elsewhere. The first frame of p_field is set to zero to anchor the spatial-slope channel:

$$p_{\text{field}}[:, 0] = \mathbf{0}, \quad p_{\text{field}}[:, 1] = p[:, 1], \quad p_{\text{field}}[:, t] = \mathbf{0} \text{ for } t \ge 2,$$
 (11)

$$q_{\text{field}}[:,0] = q[:,0], \quad q_{\text{field}}[:,1] = q[:,1], \quad q_{\text{field}}[:,t] = 0 \text{ for } t \ge 2.$$
 (12)

Normalization. To harmonize dynamic range, we apply channelwise min–max normalization to $[\ell, u]$ with $\ell = -1$ and u = 1,

$$\widetilde{X} = \ell + \frac{u - \ell}{X_{\text{max}} - X_{\text{min}} + \epsilon} (X - X_{\text{min}}), \qquad X \in \{\text{full_p}, \text{full_q}\},$$
(13)

and use the same affine map for the corresponding conditioning frames.

Algorithm 1 Ground-Truth Data Generation (create_string_dataset v3.0, z-space, s-displacement)

- 1: Set $N_z^{\text{fine}} \leftarrow 4N_z$ and $N_t^{\text{fine}} \leftarrow 4N_t$
- 2: **for** each sample **do**
- 3: Sample $\{a_n, \phi_n\}_{n=1}^{N_{\text{m}}}$ and construct s_0, w_0 via (10)
- 4: Integrate (7) on the fine grid to obtain $s^{\text{fine}}(z_i, t_i)$
- 5: Compute $p^{\text{fine}} = \partial_z s^{\text{fine}}$ and $q^{\text{fine}} = \partial_t s^{\text{fine}}$ using centered differences
- 6: Downsample p^{fine} , q^{fine} to $p, q \in \mathbb{R}^{N_z \times N_t}$
- 7: Set targets full_p $\leftarrow p$ and full_q $\leftarrow q$
- 8: Form conditioning p_field, q_field with the first two frames and zeros elsewhere, enforcing p_field[:, 0] = 0
- 9: Apply channelwise normalization and write tensors to disk
- 10: **end for**

A.2 SYNTHESIZE DATASET USING MEAN PREDICTION OF GP-DPHS

This section describes how the version 4 data generator constructs spatiotemporal training pairs by simulating the mean field dynamics implied by a trained Gaussian–Process distributed Port–Hamiltonian system. The generator replaces the analytical wave operator with the posterior mean of two Gaussian Processes that approximate the Hamiltonian gradients and then integrates the induced first–order evolution to produce full fields of p and q.

Learned energy gradients and induced evolution Let u(x,t) denote displacement on $x \in [0,L]$ and $t \in [0,T]$. The representation uses

$$p(x,t) = \partial_t u(x,t), \qquad q(x,t) = \partial_x u(x,t),$$
 (14)

stacked channelwise into x(x,t) = [p(x,t), q(x,t)]. The GP dPHS module comprises two Gaussian Processes trained on pairs (p,q) to regress the energy gradients $g_p = \partial E/\partial p$ and $g_q = \partial E/\partial q$. Denote their posterior means by

$$\mu_p(p,q) = \mathbb{E}[g_p(p,q) \mid \mathcal{D}], \qquad \mu_q(p,q) = \mathbb{E}[g_q(p,q) \mid \mathcal{D}], \tag{15}$$

where \mathcal{D} is the training set of derivative–integral pairs. The distributed Port–Hamiltonian evolution induced by these learned gradients is

$$\partial_t p(x,t) = \partial_x \mu_q(p(x,t), q(x,t)), \qquad \partial_t q(x,t) = \partial_x \mu_p(p(x,t), q(x,t)), \tag{16}$$

with fixed—end constraints applied at the spatial boundaries for the p channel. Equation (16) specializes the canonical dPHS structure to the GP mean and consequently yields a learned but physically structured flow on the representation.

Space-time discretization and solver Discretize the spatial domain on S nodes with spacing Δx and the time horizon on T frames with step Δt . Let \mathbf{D}_x be the standard centered first-difference matrix on the interior nodes with Dirichlet boundary handling. Vectorize the state at time t as $\mathbf{x}(t) \in \mathbb{R}^{2S}$ with $\mathbf{x}(t) = [\mathbf{p}(t); \mathbf{q}(t)]$. The right-hand side used by the integrator is

$$\frac{\mathrm{d}}{\mathrm{d}t} \begin{bmatrix} \mathbf{p}(t) \\ \mathbf{q}(t) \end{bmatrix} = \begin{bmatrix} \mathbf{D}_x \, \mu_q(\mathbf{p}(t), \mathbf{q}(t)) \\ \mathbf{D}_x \, \mu_p(\mathbf{p}(t), \mathbf{q}(t)) \end{bmatrix},\tag{17}$$

where μ_p and μ_q are evaluated pointwise at each spatial node using the trained GP posterior means. A standard explicit adaptive ODE solver advances (17) over $[0, T\Delta t]$. After each step, boundary rows of \mathbf{p} are set to zero to enforce fixed ends, which preserves the intended physical interpretation of p at the string endpoints.

Initialization and conditioning convention The generator samples smooth, band–limited initial profiles that satisfy the boundary conditions. The convention follows the version 3 setup for compatibility with the downstream diffusion model. The first frame of the p channel is set to zero and the first two frames of the q channel are provided by the sampler. The solver then integrates (17) forward in time to obtain a complete trajectory $\{\mathbf{p}(t_j), \mathbf{q}(t_j)\}_{j=0}^{T-1}$ on the learning grid. This seeding strategy anchors the learned representation on early frames and stabilizes the subsequent generative steps.

Mean only synthesis and uncertainty handling The evolution in (17) uses the posterior means μ_p , μ_q exclusively to synthesize ground truth. This choice yields a single, coherent physical trajectory per initialization without injecting GP sampling noise, which is desirable when creating supervisory targets for representation learning. The GP predictive variances are retained as optional quality indicators for out–of–distribution detection during generation and can be logged for later analysis but do not perturb the synthesized fields.

Packaging and normalization For each realization the generator writes a four-channel tensor of shape [4, S, T],

The targets are $full_p = p$ and $full_q = q$. The conditioning channels encode the two initial time frames with zeros elsewhere and respect the initialization convention for p. A channelwise affine normalization maps the targets to a symmetric range with the same transform applied to the corresponding conditioning frames to maintain consistency.

A.3 SYNTHESIZE DATASET USING SAMPLE PREDICTION OF GP-DPHS

From limited observations to a generative physics prior. Let $\mathcal{D} = \{(\mathbf{x}_n, y_n)\}_{n=1}^N$ be a small set of observations used to train a Gaussian process distributed Port Hamiltonian system. The Gaussian process does not return a single function, it yields a posterior distribution over Hamiltonian energy functionals. We exploit this posterior to draw function realizations of the energy gradients and to simulate many physically consistent trajectories $\mathbf{x}(t,z) = [p(t,z), q(t,z)]^{\mathsf{T}}$ for diffusion training.

Random Fourier feature prior draw. Consider a real, continuous, shift invariant kernel $k_f(\cdot,\cdot)$ for the gradient field. By Bochner theory there exists a spectral density $\rho(\omega)$ such that

$$k_f(\mathbf{x}, \mathbf{x}') = \int_{\mathbb{R}^d} e^{i \boldsymbol{\omega}^\top (\mathbf{x} - \mathbf{x}')} \rho(\boldsymbol{\omega}) d\boldsymbol{\omega}.$$

We approximate k_f by a random D dimensional feature map

$$\phi(\mathbf{x}) = \sqrt{\frac{2}{D}} \left[\cos(\boldsymbol{\omega}_1^{\mathsf{T}} \mathbf{x} + \beta_1), \dots, \cos(\boldsymbol{\omega}_D^{\mathsf{T}} \mathbf{x} + \beta_D) \right]^{\mathsf{T}},$$

with $\omega_j \sim \rho$ and $\beta_j \sim \text{Uniform}[0, 2\pi]$. This gives $k_f(\mathbf{x}, \mathbf{x}') \approx \phi(\mathbf{x})^\top \phi(\mathbf{x}')$. A pathwise prior sample is then

$$f_0(\mathbf{x}) = \phi(\mathbf{x})^{\top} \mathbf{w}, \quad \mathbf{w} \sim \mathcal{N}(\mathbf{0}, \mathbf{I}),$$

which provides one random realization for the stacked energy gradients $f(\mathbf{x}) = [d\hat{E}/dp(\mathbf{x}), d\hat{E}/dq(\mathbf{x})]^{\top}$.

Posterior correction on a finite set. Let $X = [\mathbf{x}_1, \dots, \mathbf{x}_N]$ collect the training inputs and let \mathbf{y} collect the targets. Denote the learned mean by $\mu_f(\cdot)$. Define the covariance blocks

$$\mathbf{C}_{XX} = \left[k_f(\mathbf{x}_i, \mathbf{x}_j) \right]_{ij}, \quad \mathbf{C}_{\star X} = \left[k_f(\mathbf{x}_i^{\star}, \mathbf{x}_j) \right]_{ij}, \quad \mathbf{C}_{\star \star} = \left[k_f(\mathbf{x}_i^{\star}, \mathbf{x}_j^{\star}) \right]_{ij},$$

for any query set $X_{\star} = \{\mathbf{x}_{j}^{\star}\}_{j=1}^{N_{\star}}$. The random Fourier feature draw induces the vector $f_{0}(X)$ and its evaluation on X_{\star} , written $f_{0}(X_{\star})$. A function sample from the posterior on X_{\star} is obtained by the exact conditioning correction

$$f(\mathbf{x}^{\star}) = \mu_f(\mathbf{x}^{\star}) + f_0(\mathbf{x}^{\star}) + \mathbf{C}_{\star X} (\mathbf{C}_{XX} + \sigma_n^2 \mathbf{I})^{-1} (\mathbf{y} - \mu_f(X) - f_0(X)), \quad (19)$$

applied entrywise to both gradient components. Equation (19) warps the prior draw so that it agrees with the observations in a kernel consistent manner, and it yields an exact posterior sample in the finite dimensional sense induced by X and X_{\star} .

Insertion into the distributed Port Hamiltonian dynamics. The sampled gradients define the variational derivative $\delta_{\mathbf{x}}\hat{\mathcal{H}}(\cdot) = \left[d\hat{E}/dp(\cdot),\,d\hat{E}/dq(\cdot)\right]^{\top}$. On the spatial grid we assemble the semi discrete evolution

$$\frac{d}{dt} \begin{bmatrix} \mathbf{p}(t) \\ \mathbf{q}(t) \end{bmatrix} \; = \; \mathbf{A} \; \delta_{\mathbf{x}} \hat{\mathcal{H}} \! \left(\mathbf{p}(t), \mathbf{q}(t) \right) \; + \; \mathbf{B} \, \mathbf{u}(t),$$

where $\bf A$ is the discrete representation of J-R and boundary conditions, and $\bf B$ maps inputs. The right hand side is evaluated by applying centered differences in the interior and consistent one sided stencils at the boundaries to the sampled gradient fields. With initial state fixed by the first two frames, we integrate in time with an adaptive Runge Kutta scheme to obtain the trajectories

$$\label{eq:full_p} \begin{split} \text{full_p} &= \{\mathbf{p}(t_i)\}_{i=1}^{N_t}, \qquad \text{full_q} &= \{\mathbf{q}(t_i)\}_{i=1}^{N_t}. \end{split}$$

Assembly of conditioning and targets. The conditioning channels keep only the first two frames,

$$p_{field}(:,:,1:2) = full_p(:,:,1:2),$$
 $q_{field}(:,:,1:2) = full_q(:,:,1:2),$

and are zero elsewhere. Stacking [p_field, full_p, q_field, full_q] yields a tensor of shape $[4, N_z, N_t]$ that matches the diffusion model interface.

Why this sample based generator helps representation learning. Drawing $\delta_{\mathbf{x}}\hat{\mathcal{H}}$ from the posterior produces a family of Hamiltonian consistent vector fields that reflect epistemic uncertainty learned from \mathcal{D} . The resulting collection of simulated trajectories covers a diverse yet physically structured region of the state space. This enlarged dataset serves as supervision for the diffusion objective, which we further weight by the predictive uncertainty, thereby aligning the learned score field with the Port Hamiltonian manifold while remaining data efficient.

Implementation notes in v5.0. The code fixes the trained hyperparameters, constructs the random Fourier feature map, draws w to obtain f_0 , and applies the posterior correction in (19) on the grid required by the discrete operator. Each dataset shard records the random seeds, solver tolerances, grid sizes (N_z, N_t) , and identifiers of the hyperparameters to ensure exact reproducibility of the sampled gradient fields and of the generated trajectories.

A.4 DISPLACEMENT RECONSTRUCTION FROM (p,q) AND VALIDATION PROTOCOLS

State, operators, and learned surrogates. On a spatial grid $\mathcal Z$ and discrete time index $t=0,\dots,T$, the port-Hamiltonian state is $(p_t(z),q_t(z))$. The GP-dPHS learns the Hamiltonian gradients as functions on the grid, yielding surrogates $\widehat{g}_p(p,q) \approx \partial H/\partial p$ and $\widehat{g}_q(p,q) \approx \partial H/\partial q$ (implemented by the two trained heads loaded from model_dp_trained.pth and model_dq_trained.pth). In the canonical wave-form system, the continuous-time dynamics are $\dot{q}=\partial H/\partial p$ and $\dot{p}=-\partial H/\partial q$; we therefore define $\widehat{dq}(p,q):=\widehat{g}_p(p,q)$ and $\widehat{dp}(p,q):=-\widehat{g}_q(p,q)$. Boundary handling follows the PDE module used during training (Dirichlet by default in our code), and the time step Δt is read from the dataset metadata.

Displacement reconstruction (rollout). Given two initial frames (p_0, q_0) and (p_1, q_1) on \mathcal{Z} , we reconstruct the entire displacement trajectory $\{q_t\}_{t=2}^T$ by iterating an explicit, symplectic first-order update (vectorized over $z \in \mathcal{Z}$):

$$q_{t+1} = q_t + \Delta t \, \widehat{dq}(p_t, q_t), \qquad p_{t+1} = p_t + \Delta t \, \widehat{dp}(p_t, q_t), \qquad t = 1, \dots, T-1.$$

In practice, we: (i) load the GP-dPHS checkpoints and the dataset item containing *initial* two frames (p_init, q_init); (ii) standardize/unstardardize using the same statistics as training; (iii) loop the update above for T-2 steps; (iv) enforce the boundary condition after each step. The reconstructed displacement is the sequence $\{q_t\}$.

How this appears in the codebase. Data are formatted as four channels (p_full, p_init, q_full, q_init) by the dataset scripts (create_string_dataset_v5.py). The GP models are defined and loaded from train_gp_phs_v35.py, while the port-Hamiltonian residuals and utilities reside in pde.py and residuals_string.py. The diffusion model (unet_model.py with sampling utilities in denoising_utils.py/main.py) consumes the same conditioning (p_init, q_init) to generate trajectory samples that are evaluated against the ground truth produced by the GP-dPHS simulator.

Validation protocol. We validate two aspects: (A) the *physics fidelity* of GP-dPHS rollouts; (B) the *data efficiency and accuracy* of the diffusion model trained on GP-dPHS trajectories.

1. **GP-dPHS accuracy.** For a set of random initializations, compare $\{q_t\}$ reconstructed by the GP-dPHS integrator to the reference simulator (same grid and Δt). Report MSE scores.

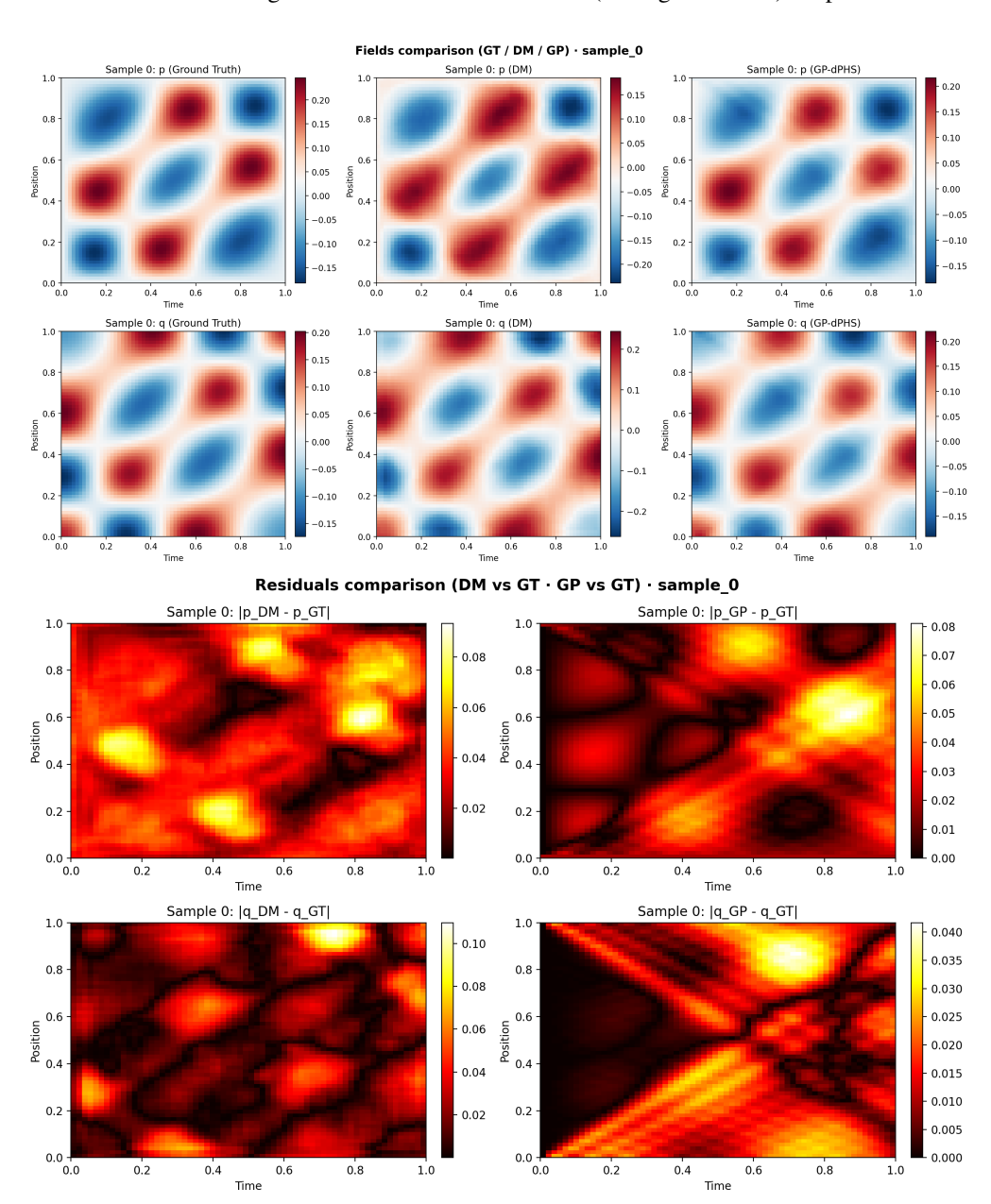


Figure 5: Validation of GP-dPHS performance and PHDME performance. The left column is the ground-truth dynamics generated by A.1, the middle column is the forecast made by the proposed method, and the last column is the GP-dPHS prediction based on the initial conditions. Key takeaway: Both GP-dPHS and PHDME have learned the correct dynamic patterns, but not 100% perfect. The red residual comparsion figures show the differences, notice that the magnitude of the residual is very low.

Reconstruction of the displacement using the generated states. Train the diffusion model in using the state and state derivatives of the system, which is the key to getting

rid of the exact function of movements. We want to validate that the proposed method can reconstruct the displacement over time by using the predicted state.

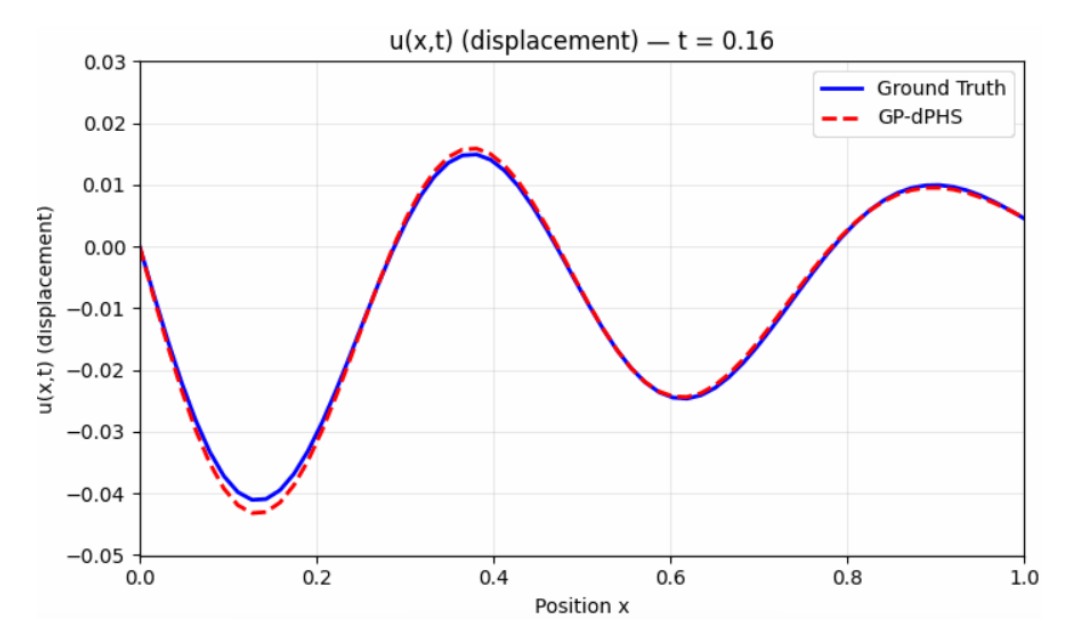


Figure 6: This is the reconstruction based on the derivative field, the blue line is the movement (displacement) of the soft string system using a faithful physics simulator. The red dot line is the one reconstructed based on the derivative field using the rollout that has been mentioned above. Key takeaway: The state and state derivative method is applicable to the physics-informed machine learning.

Notes for exact reproducibility. Use the saved checkpoints $model_dp_trained.pth$ and $model_dq_trained.pth$; read metadata.json for Δt , grid size, and normalization; ensure the same boundary operator as in training; and keep the discretization identical to the equations above so that the reconstruction and training distributions match. You can run the $train_gp_phs_v35.py$ file to get the GIF of the reconstruction over time.

A.5 REPRESENTATION LEARNING OF PHDME

A central component of PHDME is the use of Gaussian Processes to learn the energy representation of the distributed port-Hamiltonian string system from limited data. Unlike purely data-driven models that fit trajectories directly, our GP-dPHS surrogates approximate the underlying gradients of the Hamiltonian, dE/dp and dE/dq, providing a structured representation aligned with physical laws.

Learning energy gradients. The training data consist of spatiotemporal fields of momentum p and strain q generated from the wave system. From these, we compute integrated derivatives that serve as training targets for the GP models. Two Gaussian Processes are trained jointly: one learns the mapping $(p,q)\mapsto dE/dp$ and the other $(p,q)\mapsto dE/dq$, thereby embedding the system into an implicit energy functional. This construction encodes the Hamiltonian structure directly into the representation space.

Visualization of learned surfaces. Figure 7 and Figure 8 show the learned GP surfaces for dE/dp and dE/dq, respectively, overlaid with the training data. Even with only 1640 training data points drawn from a single Hamiltonian-consistent trajectory, the GP recovers smooth and coherent energy gradients across the (p,q) domain. This confirms that the representation is not tied to specific trajectories, but generalizes across state space.

Role in PHDME. These GP-learned energy gradients form the backbone of the physics-informed diffusion model. Instead of constraining the generative model with explicit PDE coefficients,

PHDME leverages the GP posterior as a flexible representation of admissible energy functionals. During diffusion training, the GP structure enters the physics loss to guide denoising steps toward physically consistent dynamics. This tight coupling ensures that the learned latent dynamics reflect both data evidence and energy-based physics, enabling sharper generalization to unseen conditions.

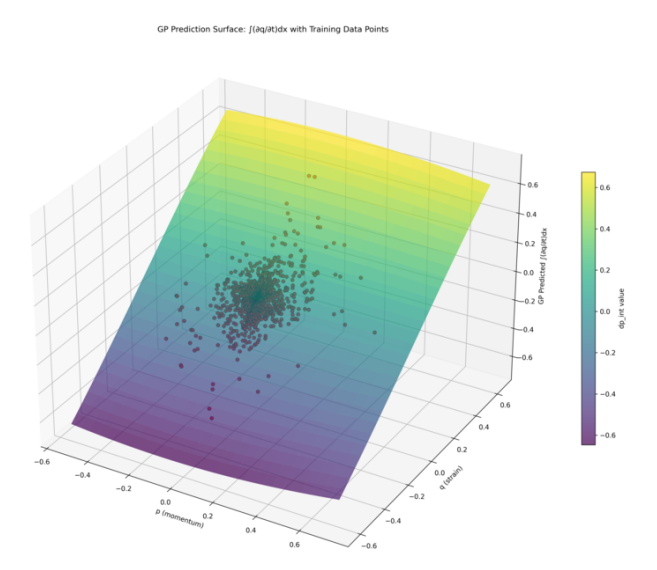


Figure 7: GP-learned representation of dE/dp (partial derivative of energy) with training data points. The limited observations lie on the surface of the GP plane, indicating the correct and smooth energy representation of the system.

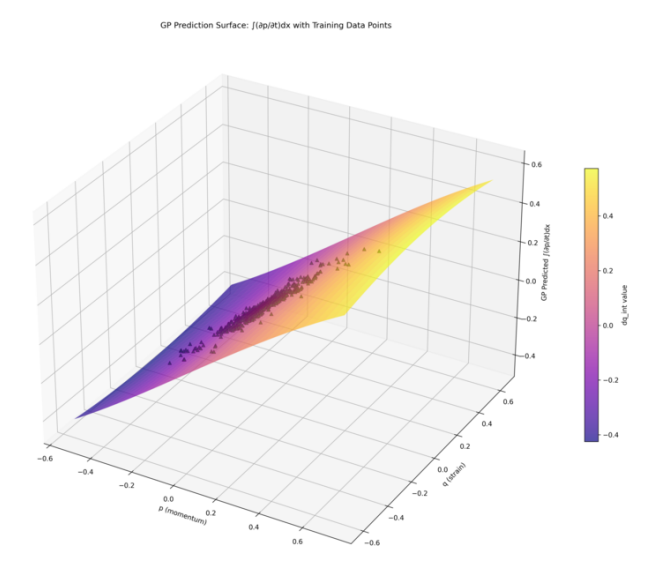


Figure 8: GP-learned representation of dE/dq (partial derivatives of energy) with training data points. The limited observations lie on the surface of the GP plane, indicating the correct and smooth energy representation of the system.

A.5.1 FUTHER DISCUSSION AND LIMITATIONS

Limitations under extreme scales. While the GP-based representation is robust to moderate data scarcity, it exhibits limitations when the dynamics evolve near extremely small state magnitudes. In

 these regimes, the training data provide only sparse coverage of the (p,q) space, and the GP posterior surfaces tend to flatten, resulting in poor approximation of the true energy gradients. Consequently, when the diffusion model is conditioned on such representations, generated samples may fail to capture fine-scale oscillatory behavior. This effect is visible in the tails of the learned surfaces, where variance grows and predictions become less structured.

Relative performance. Despite these limitations, PHDME consistently outperforms non-physics baselines and ablated variants. Even when extreme scales introduce local inaccuracies, the GP-informed energy representation provides global structural regularization, preventing the generative process from drifting into unphysical states. As a result, the model produces sharper and more reliable forecasts on average, while the baselines either overfit to data trajectories or violate physical constraints. Thus, although failure cases exist at vanishingly small state magnitudes, the method achieves overall superior representation quality and downstream predictive performance.

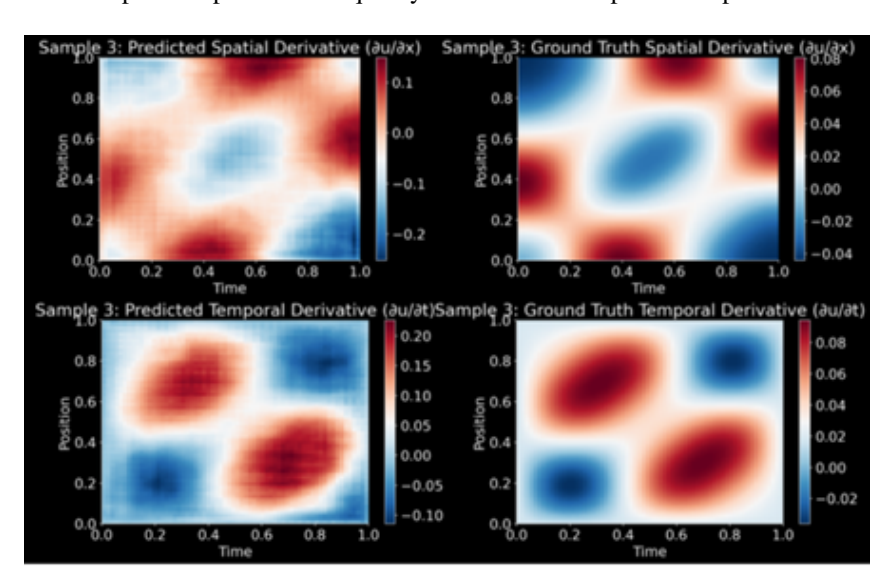


Figure 9: The left side is the dynamic generated by the data-driven diffusion model, while the right side is the ground truth dynamics generated by the physically-faithful simulator. It's obvious that the pure-data-driven method compromises its accuracy under the initial conditions that have never been met before.

And besides being reported in the experimental part, we would also like to visualize the conformal prediction using the ranked score.

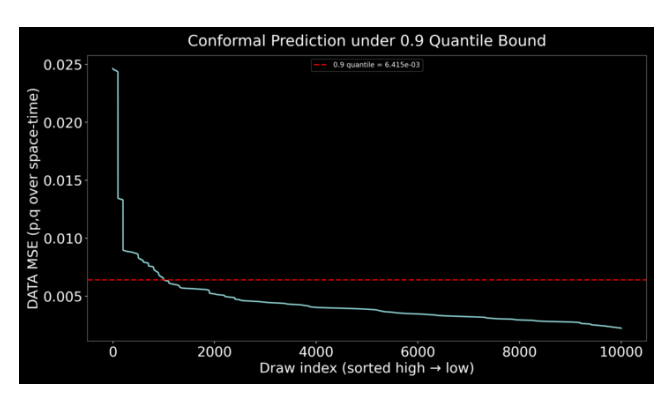


Figure 10: The visualized conformal boundary under 90% of guarantees.